



Synthesis and characterization of Mo-blue-based CoMo/Al₂O₃ catalysts

A. W. Gutiérrez^a • J. Escobar^{b*} • P. del Ángel^a •
M. C. Barrera^b • V. Santes^c • C. E. Santolalla^c • D. A. Solís-Casados^d

^aInstituto Mexicano del Petróleo, Eje Central Lázaro Cárdenas 152, San Bartolo Atepehuacan,
G.A. Madero, Cd. de México, 07730, México

^bFacultad de Ciencias Químicas-Centro de Investigación en Recursos Energéticos y Sustentables, Universidad Veracruzana,
Campus Coatzacoalcos, Av. Universidad km. 7.5, Col. Santa Isabel, Coatzacoalcos, Veracruz, 96538, México

^cDepartamento de Biociencias e Ingeniería, Centro Interdisciplinario de Investigaciones y Estudios en Medio Ambiente
y Desarrollo (CIEMAD), Instituto Politécnico Nacional, C.P. 07340, Ciudad de México, México

^dUniversidad Autónoma del Estado de México, Centro Conjunto de Investigación en Química Sustentable. Km. 14.5 Carretera
Toluca-Atlacomulco, Toluca, Estado de México, 50200, México

Received 06 09 2020; accepted 01 20 2022

Available 06 30 2022

Abstract: Saccharose (SA) and citric acid (CA) were used as additives in P-doped CoMo/Al₂O₃ catalysts (Mo, Co and P at 12, 3, and 1.6 wt%, respectively). One-pot impregnating solutions were prepared by MoO₃ digestion in aqueous H₃PO₄, followed by C₄H₆CoO₄•4H₂O addition. Organics were added (SA/Co=1, CA/Co=2) at two different preparation stages to assess the effect of that step on catalysts properties. Method I: SA or CA was added in as-prepared Co-Mo-P impregnating solution, followed by pore-filling impregnation of alumina support. Method II: SA or CA at aforementioned concentrations was impregnated on the pristine carrier, followed by drying (120 °C, 2 h). Co-Mo-P phases were further deposited on modified supports through corresponding one-pot solutions. All materials were dried (120 °C) but not calcined. Cobalt complexation by CA and Mo-blue ligand to metal charge transfer complex formation (SA-modified solids) were identified (UV-vis, oxidic samples). Partially reduced molybdenum (Mo⁶⁺ => Mo⁵⁺, by XPS) was observed after organics addition that being more evident in SA-modified solids. Materials were gas-phase sulfided (H₂S/H₂ 10%, 400 °C, 2 h) then studied by HR-TEM. Co-Mo-P phases impregnation in one-pot solution simultaneously deposited with SA rendered the materials of the highest MoS₂ dispersion.

Keywords: Saccharose, citric acid, complexation, Mo-blue, CoMo/Al₂O₃

*Corresponding author.

E-mail address: jeaguila@imp.mx (J. Escobar).

Peer Review under the responsibility of Universidad Nacional Autónoma de México.

1. Introduction

Considering renewable resources (e.g., solar and eolic, etc.), biomass is the only organic carbon raw material that could be converted to value-added products. Along past few decades, research on the production of value-added chemicals, alternative fuels and platform compounds from lignin has grown rapidly attesting its importance in biorefineries schemes. Lignin accounts for 10-35% by weight, up to 40% by energy in biomass. Then, chemical and fuels production from lignin could significantly improve the economics of biorefinery process (Li et al., 2015). Hydrodeoxygenation (HDO) is the most efficient method for bio-oil upgrading as it allows to decrease original oxygen content (typically 10-40 wt%) to essentially total elimination under operating conditions similar to those used in commercial hydrotreaters for the production of oil-derived diesel. High oxygen content in raw biomass derived-oils imparts undesirable physical and chemical properties as high viscosity, corrosiveness and thermal instability among others, precluding their direct use (Bui et al., 2011a). Guaiacol (GUA) well represents aromatic oxygenated species present in biomass pyrolysis oil (Qi et al., 2007) or lignin depolymerization products (Chio et al., 2019). Several investigations on GUA and other oxygenates HDO have been addressed by using alumina-supported CoMo (Bui et al., 2011b; Bui et al., 2009; Tavizón-Pozos et al., 2019) or NiMo (Kaluža et al., 2019; Lin et al., 2011) sulfided formulations finding interesting results. Thus, obtaining CoMo/Al₂O₃ solids of enhanced catalytic properties (activity and selectivity, stability under reaction conditions, etc.) is always demanded.

The use of organic additives during hydrodesulfurization (HDS) catalysts preparation has resulted in enhanced organo-S removal activity during oil-derived streams processing. It is well-accepted that complexing organic compounds could enhance Mo-promoter (Ni or/and Co) interaction during catalyst sulfiding that resulting in materials of increased HDS activity (Lélias et al., 2009; van Haandel et al., 2017). Chelation allows promoter sulfidation to temperatures high enough to permit efficient integration of sulfidic Co or/and Ni species to then already formed MoS₂ (or WS₂), thus optimizing promoted phases ("NiMo(W)S" or "CoMo(W)S") formation. On the other hand, regarding non-complexing species as HDS catalysts additive no general consensus on the origin of their beneficial influence has been reached so far. It appears that enhanced HDS activity could be originated by a number of factors (Escobar et al., 2009; Escobar et al., 2018; Nicosia & Prins, 2005a; Nicosia & Prins, 2005b). For instance, for glycols-modified P-doped CoMo/Al₂O₃ formulations it has been proposed that interaction of organic additive with both basic OH groups and coordinatively unsaturated Al³⁺ sites on alumina surface could partially prevent Co diphosphopentamolybdate Strandberg heteropolyanions (Catita et al., 2017) decomposition during their deposition on the

carrier (Nicosia & Prins, 2005a). Thus, close proximity of Co and Mo in those complexes could result in increased amount of highly active mixed "CoMoS phase" during sulfiding. Beneficial influence of ethylene glycol when simultaneously impregnated with Ni, Mo and P over alumina support has been documented (Escobar et al., 2009) as well. Again, enhanced formation of well-promoted "NiMoS" phase due to decreased support-impregnated Mo interaction was invoked to explain enhanced activity in both dibenzothiophene (DBT) and straight-run gas oil HDS. Recently, we reported (Escobar et al., 2018) on using saccharose as precursor of Mo⁶⁺ species reducing agents (monosaccharides) rendering Mo-blue species that after sulfiding resulted in alumina-supported P-doped NiMo catalyst of improved HDS. Under synthesis conditions and by reducing Mo⁶⁺ species monosaccharides could be converted to complexing organic acids that could possibly interact with Ni promoter being also able to decrease deposited species-carrier interaction by carbonaceous deposits formation. Then, it seems that positive influence of non-complexing organic additives on the S-removal activity of corresponding catalysts could be related to several independent phenomena.

Comparative studies (Vatutina et al., 2020) using CoMo formulations over multi-walled carbon nanotubes (MWCNT) found that chelating citric acid was more efficient than diethylene glycol addition in improving DBT HDS and quinoline hydrodenitrogenation. Decreased support-Mo interaction provoked by the later additive was not very effective in promoting activity as impregnated phases were not strongly bonded to MWCNT. On the other hand, triethylene glycol and thioglycolic acid addition resulted in decreased active phase aggregation (diminished MoS₂ slab length and stacking in CoMoP/Al₂O₃ catalysts) that was reflected in augmented activity in both toluene hydrogenation and straight-run gas oil-light cycle oil mixture HDS (Humbert et al., 2021). Clearly, the effect of various organic additives, either chelating or not, on HDS catalysts performance depends upon specific interactions with the deposited phases (Mo, W, etc.) and promoters (Ni, Co, etc.) under distinctive preparation conditions (concentration, pH, type of support, etc.). MoS₂ particles morphology, as determined by organics addition, could also strongly influence selectivity by exposing preferential edges. For example, sulfur vacancies on S-edge of CoMoS₂ catalysts had higher selectivity for heteroatoms removal over that to hydrogenation (Zheng et al., 2021).

During the present investigation Al₂O₃-supported P-doped CoMo catalysts were prepared by adding complexing and non-chelating organic modifiers (CA and SA, respectively) at two different preparation stages. Oxidic materials were studied by using several textural, structural and surface characterization techniques. Also, corresponding sulfided catalysts were studied by HR-TEM to determine their morphology (MoS₂ slabs length and stacking).

2. Materials and methods

2.1. Catalysts synthesis

Al₂O₃ powder was obtained by annealing (500 °C, 5 h under static air) commercial Pural SB sol-gel pseudo-boehmite (from Sasol, obtained from Al-alkoxides). Oxidic catalyst precursors were prepared by one-pot impregnation of Mo, Co and phosphorous (at 12, 3 and 1.6 wt%, respectively) by pore-filling through an aqueous solution where MoO₃ was digested (at ~80 °C) in diluted H₃PO₄. H₂O in excess (typically 250 ml of starting solution to impregnate 5 g of alumina carrier) was used to accelerate dissolution and digestion of molybdenum salt. After ~4 h cobalt acetate (C₄H₆CoO₄•4H₂O) was added, the solution being then digested by additional 4 h (~80 °C). The described one-pot impregnation method was chosen as it constitutes a readily scalable methodology used during commercial catalysts preparation. It includes cheap industrial precursors easily affordable for industrial catalysts manufacturing. To determine the influence of organic modifiers (saccharose, SA, at SA/Co=1 (Escobar et al., 2018) or citric acid, CA, at CA/Co=2 mol ratio (Escobar et al., 2008) added at different preparation steps two methodologies were followed. In method I SA or CA were directly added to the already prepared Co-Mo-P aqueous solution (at ~80 °C, pH~2) to simultaneously (one-pot) impregnate the corresponding amount of Al₂O₃ carrier. Immediate color change from wine-color to almost black (signaling complexes formation) was observed for the SA-modified impregnating solution. Impregnated materials were allowed to stand overnight at room temperature in a capped beaker to permit diffusion of deposited species into the support porous network. Materials were dried at 120 °C (2 h), samples SAI and CAI, respectively. Regarding the second preparation methodology, the carrier was firstly impregnated by pore-filling with aqueous SA or CA solutions at concentration again corresponding to SA/Co= 1 and CA/Co=2 mol ratio, solids being then dried at aforementioned conditions. Subsequently, Co-Mo-P phases were simultaneously deposited over the modified supports by pore-filling impregnation. Resulting materials were then dried at 120 °C (2 h), samples SAII and CAII. To preserve organic additive integrity high-temperature annealing was avoided in all cases. A reference alumina-supported Co-Mo-P impregnated reference formulation was also prepared. This solid was dried (120 °C, 2 h, sample CM_d), a portion being calcined at 400 °C (4 h, solid CM_c). Supported sulfidic catalysts were obtained by submitting approximately 0.3 g of ground (U.S. mesh size 80-100, ~165 μm average particle diameter) impregnated precursors to treatment at 400 °C (heating rate 6 °C min⁻¹) under H₂/H₂S (Praxair) at 50 ml min⁻¹/6 ml min⁻¹ ratio during 2 h.

2.2. Materials characterization

Textural properties of support and Co-Mo-P impregnated solids were determined by N₂ physisorption (at -196 °C) in a Micromeritics Tristar II 3020 apparatus after ultra-high vacuum degassing at ~300 °C for 2 h. Surface area and pore size distribution of studied materials were determined by BET and BJH (adsorption branch data) methods, respectively. Thermogravimetric analysis (TGA) of impregnated samples were carried out through a TA instruments Q2000 equipment. 15-50 mg samples were analyzed in the 30-1000 °C temperature range (heating ramp of 0.166 °C s⁻¹). Differential thermogravimetric (DTG) profiles were obtained through derivatives of corresponding TG curves. Also, differential scanning calorimetry (DSC) profiles of various samples prepared with organic additive were obtained through a Q2000 equipment from TA instruments.

UV-vis diffuse reflectance spectroscopy (DRS) analyses of impregnated samples were carried out in a Perkin Elmer Lambda 35 spectrophotometer equipped with integration sphere. Spectra were acquired in the wavelength range from 200 to 1100 nm. Spectralon signal was subtracted as baseline. Supported Co-Mo samples (~100 mg put in a quartz cell) were studied by temperature programmed reduction (TPR, in the 25-850 °C range, 10 °C/min heating rate) using an ICID SRyC-2 apparatus equipped with a thermal conductivity detector. To that end, a H₂/N₂ mixture (at 1/9 L/L, 20 cm³/min total flow) was used. X-ray photoelectron spectroscopy (XPS) analysis was carried out using a K-alpha Thermo Fischer Scientific spectrometer with a monochromatic Al K_α radiation (1486.6 eV) as X-ray source that was micro-focused at the source to give a 400 microns diameter spot size on the sample. XPS high-resolution spectra were collected using analyzer pass energies of 20 eV. To compensate effects related with charge shift, C1s peak at 284.6 eV was used as internal standard.

Sulfided catalyst (see 2.1. Catalysts synthesis section) were characterized by high-resolution transmission electron microscopy (HRTEM) performed in a Titan 80-300 microscope with a Schottky-type field emission gun operating at 300 kV. The point resolution and the information limit were better than 0.085 nm. HRTEM digital images were obtained using a CCD camera and Digital Micrograph Software from GATAN. In order to prepare the materials for observation, the powder samples were ultrasonically dispersed in ethanol and supported on lacey carbon coated copper grids. GATAN™ software was used during determination of MoS₂ particles morphology (slab length and stacking degree). Average length and stacking number of MoS₂ slabs ($L_{avg.}$ and $N_{avg.}$, respectively) were statistically estimated through measurements carried out in ~300 MoS₂ slabs per sample through the following equations:

$$L_{avg.} = \frac{\sum_{i=1..t} n_i L_i}{\sum_{i=1..t} n} \quad (1)$$

$$N_{avg.} = \frac{\sum_{i=1..t} n_i N_i}{\sum_{i=1..t} n} \quad (2)$$

where n_i is the number of slabs in a given range of length or stacking (L_i and N_i , respectively) and t is the total number of analyzed MoS₂ slabs. MoS₂ phase aspect ratio, Ar_{MoS_2} (1/nm), was defined as:

$$Ar_{MoS_2} = \frac{N_{avg.}}{L_{avg.}} \quad (3)$$

MoS₂ edge-to-corner ratio (f_e/f_c)_{MoS₂} was calculated through the following equation:

$$\left(\frac{f_e}{f_c}\right)_{MoS_2} = \frac{Mo_e}{Mo_c} = \frac{10 \times L_{avg.} / 3.2 - 3}{2} \quad (4)$$

where Mo_e and Mo_c stands for Mo⁴⁺ atoms in edges and corners of hexagonal MoS₂ particles, respectively.

Dispersion of molybdenum atoms in MoS₂ crystals was determined from corresponding hexagonal geometrical model (Kasztelan et al., 1984). Thus:

$$D_{MoS_2} = \frac{Mo_e + Mo_c}{Mo_t} = \frac{\sum_{i=1..t} 6n_i - 6}{\sum_{i=1..t} 3n_i^2 - 3n_i + 1} \quad (5)$$

where D_{MoS_2} is MoS₂ dispersion, Mo_e and Mo_c as previously defined meanwhile Mo_t stands for total molybdenum atoms (as determined by slabs size); n_i is the number of atoms along one side of a molybdenum sulfide slab as determined from its length, $L = 0.316 \times (2n_i - 1)$, in nm, and t is the total number of slabs analyzed from HR-TEM corresponding micrographs during the statistical counting. Interesting correlations between MoS₂ particles morphology (slab length and stacking) and their activity and selectivity in HDO reactions have been reported in the past (Liu et al., 2018; Wu et al., 2016; Wu et al., 2019 Yang et al., 2008).

3. Results and discussion

3.1. Materials textural characterization

Textural analyses of samples modified by organic additives were not carried out as presence of those agents in non-calcined solids precluded efficient parameters determination. N₂ physisorption isotherms (at 196 °C) of alumina support and corresponding impregnated materials dried and calcined (CM_d and CM_c, respectively) belonged to type IV, according to IUPAC classification (Figure S1) (Leofanti et al., 1998). Adsorbed N₂ volume clearly decreased after impregnated phase deposition that effect being more evident for the dried sample where remains from impregnation step could exist on the carrier surface. All studied solids had type H1 hysteresis, characteristic of materials consisting of particles crossed by

nearly cylindrical channels or made by aggregation (consolidated) or agglomeration (unconsolidated) of spheroidal particles. Surface area (S_{gBET}), pore volume (V_p), and average pore diameter (D_p , assuming cylindrical pores) of solids studied are shown in Table S1. Loss of S_{gBET} of CM_c sample (respecting that of bare Al₂O₃ support) was higher than expected by assuming homogeneous deposition of oxidic non-porous impregnated phases (around 0.267 g g⁻¹ of support) where a final surface area of ~183 m² g⁻¹ could be expected (instead of 149 m² g⁻¹ actually determined). That suggested some partial plugging of the carrier smaller pores where ~19% of pristine support surface area was lost after oxidic Co-Mo-P phases deposition. Expectably, that loss was much higher for the dried impregnated solid CM_d (31%). To determine which pore size distribution profile (PSD, from BJH methodology) obtained by using either adsorption or desorption data branch better fit the actual ones, corresponding cumulative surface area values were compared to those obtained through the BET method. Values from adsorption branch data, $S_{gBJH,A}$, were closest to S_{gBET} ones (Table S1). Thus, PSD profiles from those data were deemed the most suitable in describing the actual porous network, Figure S2. Pores of diameter <4.5 nm present in the pristine alumina carrier were almost totally absent in CM_c profile after Co-Mo-P phases deposition in full agreement with the surface area loss as to that of the Al₂O₃ support (Table S1). For impregnated materials shift of hysteresis closing to higher relative pressure (see Figure S1) was in full agreement with smaller pores elimination. CM_c PSD profile shifted to ~9.4 nm as to that of corresponding support (maximum at ~8.4 nm). Pore dimensions of our impregnated materials seemed to be adequate for their potential application as catalysts for guaiacol (kinetic diameter ~0.67 nm Lee et al. (2016) hydrodeoxygenation where effective reactants/products pore diffusivity strongly depends on pore size, porosity and tortuosity of catalytic particles porous network.

3.2. Thermal analysis (TG-DTG-DSC) of impregnated solids

For all studied materials weight losses up to 100 °C were attributable to water evaporation, Figure S3. The main losses for solids modified by organic additives after H₂O elimination are shown in Table S2. Temperature ranges for various weight losses were based on corresponding DTG profiles (Figure 1). CAI and CAII had decomposition/combustion steps at similar temperature intervals (Table S2) in spite of higher weight losses observed for the latter. This trend was alike to that previously registered for Al₂O₃-supported NiMo formulations where enhanced losses were observed for the sample where citric acid was impregnated over the pristine carrier prior to Ni-Mo-P phases deposition (Escobar et al., 2017) suggesting higher carbonaceous remains-support interaction in the CAII formulation.

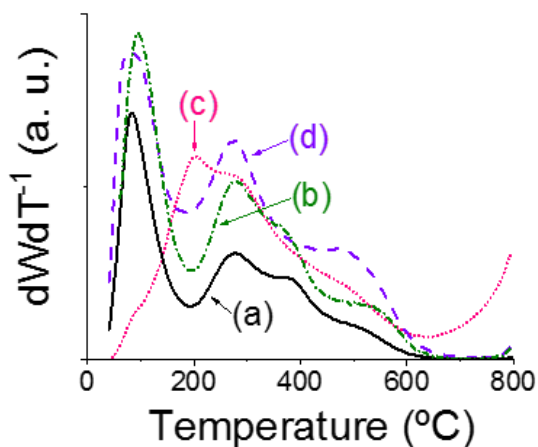


Figure 1. Differential thermogravimetric analysis profiles of various alumina-supported Co-Mo-P impregnated materials prepared with organic additive. (a): CAI; (b): CAII; (c): SAI; (d): SAII.

Under the highly acidic (pH~2) conditions of solutions used during CAI impregnation weakly acidic CA (pK_a values of 3.1, 4.7, and 6.4, for first, second and third ionization, respectively) could hardly be deprotonated that precluding interaction of acetate moieties with coordinatively unsaturated sites of surface Al^{3+} cations. Losses between 100 and 280 °C could include contributions from support dehydroxylation (surface and structural OH groups (Escobar et al., 2000) elimination of water coordinatively bonded to cobalt acetate (Grimes & Fitch, 1991) and acetates decomposition as well. Combustion of organic remains strongly bonded to the carrier could provoke the losses observed at higher temperature. Onset of signal at 780 °C for CAII absent in CAI (DTG profiles, Figure 1), could be attributable to MoO_3 melting/sublimation (Braun et al., 2005) pointing out to Mo^{6+} species of decreased interaction with the support as to those over CAI. Although SAII DTG profile (Figure 1) had features rather similar as to those of samples prepared with CA, SAI had distinctive features where a low temperature signal at around 205 °C was identified. Saccharose could be rapidly hydrolyzed under pH conditions of Co-Mo-P impregnating solution (SAI sample) forming glucose and fructose. Both of these monosaccharides could polymerize at the mentioned temperature (Órsi, 1973) producing oligo- and poly-saccharides that could be further decomposed by combustion at more severe conditions. Organics condensation and decomposition reactions could be accelerated by extant deposited Mo and/or Co species (Braun et al., 2005; Eggleston et al., 1996) those then taking place at lower temperature as to that observed for pure monosaccharides (Órsi, 1973). SA hydrolysis could not occur when dissolved in sole water being then the pristine disaccharide directly impregnated on the alumina carrier prior to Co-Mo-P phases deposition (solid SAII). Interestingly, in SAI

case onset of the weight loss related to MoO_3 sublimation started at lower temperature (675 °C) as to that observed for the rest of studied solids suggesting weakened Mo species-support interaction. Excepting absence of signal at ~380 °C, SAII DTG profile was very similar to those of CA samples.

Regarding DSC analysis, endothermic signal around 95-110 °C in all samples impregnated with organic additives was related to water evaporation (Stevulova et al., 2017), Figure 2. Higher intensity of that peak in CA-modified samples was in agreement with their enhanced H_2O content, as to those of solids prepared with SA (see corresponding TG analysis in Figure S2). Endothermic humps at ~165 °C in SA-containing samples (Figure 2 (a)) could be related to the disaccharide melting (Beckett et al., 2006). Exothermic signals at ~235 °C in SA-containing samples (more notable in SAII) suggested organic remains in weaker interaction with the supports as to those on CA-modified materials where that combustion inflexion was registered at higher temperature (see CAI profile, for instance), in agreement with that observed by DTG (Figure 1). Thermal decomposition of organic additives under air resulted in hydroxyls oxidation and consequently led to enhanced number of carbonyl groups and carboxylate formation (Fagerson, 1969; Stevulova et al., 2017).

Finally, exothermic signals at around ~440 °C in all samples studied fully agreed with decomposition of more stable carbonaceous deposits as also registered by corresponding DTG analyses (humps, Figure 1). In this line, decompositions at ~438 °C have been attributed to oxidation of charred residues (Stevulova et al., 2017).

3.3. UV-vis DRS spectroscopy studies

Maxima of main absorptions from UV-vis spectra of various prepared materials (Figure 3) are shown in Table 1.

Tetrahedral molybdenum ($Mo^{6+}_{(Th)}$) appeared at rather similar position for all materials (240-254 nm, column 2, Table 1) (Escobar et al., 2017) but in SAII (271 nm) suggesting then species of lower interaction with the support. $Mo^{6+}_{(Th)}$ entities characterize supported stable phases refractory to sulfiding (Blanchard et al., 1998). Although Strandberg heteropolyanions ($H_xP_2Mo_5O_{23}^{(6-x)-}$) (Catita et al., 2017) could exist in several protonation states over a wide pH range in the one-pot simultaneous impregnation solutions used they could decompose into PO_4^{3-} and molybdates due to their strong interaction with both basic OH's and Al^{3+} Lewis acid sites on Al_2O_3 surface (Kraus & Prins, 1996). However, organic moieties adsorption on the latter sites could passivate them diminishing molybdate-carrier interaction that being reflected in decreased tetrahedral Mo species. In the same line, by studying alumina-supported CoMo formulations it has been suggested (Nicosia & Prins, 2005a) that in materials prepared in the absence of glycols Mo^{6+} was mainly in tetrahedral geometry.

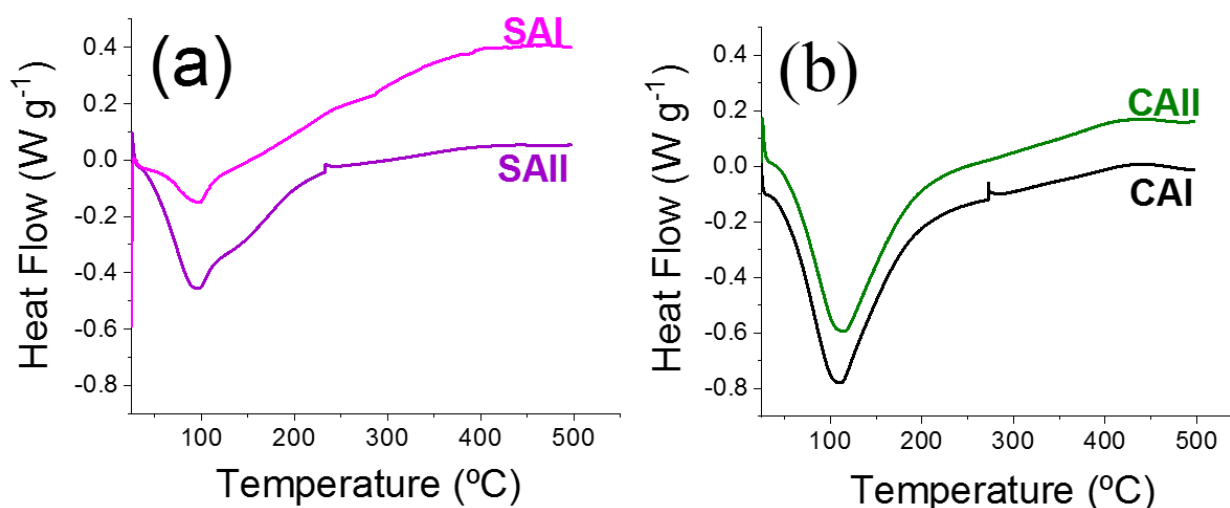


Figure 2. Differential scanning calorimetry profiles of various alumina-supported Co-Mo-P impregnated materials prepared with organic additive. (a): Samples modified by saccharose addition; (b): Samples modified by Citric acid.

Much higher variations in position (radiation energy) were observed for octahedral molybdenum $\text{Mo}^{6+}_{(\text{Oh})}$ over various studied materials (column 3, Table 1). Even more, $\text{Mo}^{6+}_{(\text{Oh})}$ of different dispersion were suggested in CM_d (maxima at 354 and 396 nm) as blue-shifted low-energy absorption edge has been related to smaller Mo_xO_y domains (Weber, 1995). Annealing could favor Mo species dispersion (Stampfl et al., 1987) but, when at severe conditions, formation of $\text{Mo}^{6+}_{(\text{Th})}$ strongly interacting with the alumina carrier could also take place. Similarly, to that found when studying alumina-supported NiMo formulations modified by CA at different preparation stages (Escobar et al., 2017), CAI and CAII had high Mo dispersion as inferred from the hypsochromic shift of low energy absorption edge as to those of the rest of solids (Figure 3). Proportion of octahedral species was enhanced in SA-modified samples and CM_d as well pointing out to decreased amount of tetrahedral ones due to diminished Mo-support interactions (Escobar et al., 2016). Regarding Co^{2+} , triplet with maxima at 540, 595 and 645 nm in CM_c characterized tetrahedral $\text{Co}^{2+}_{(\text{Th})}$ (${}^4\text{A}_2(\text{F}) \rightarrow {}^4\text{T}_1(\text{P})$ transitions) (Ramírez et al., 2000) probably in CoAl_2O_4 -like species occupying tetrahedral vacancies of alumina structure (Rinaldi et al., 2009). Conversely, absorption at 560 nm in CM_d corresponded to octahedral Co^{2+} ions ($\text{Co}^{2+}_{(\text{Oh})}$) like in inner sphere surface Co^{2+} complexes (Rinaldi et al., 2009). Also, absorptions in the 518-524 nm range in samples prepared with organic modifiers (peaks in CAI and CAII, shoulders in SAI and SAII) could probably be related to ${}^4\text{T}_{1g}(\text{F}) \rightarrow {}^4\text{T}_{1g}(\text{P})$ electronic transition of $\text{Co}^{2+}_{(\text{Oh})}$ (Xie et al., 2007) pointing out to exchange of water

ligands (in $\text{Co}(\text{H}_2\text{O})_6^{2+}$ with support hydroxyl groups signaling then surface $\text{Co-Al}_2\text{O}_3$ species formation. Thus, it appeared that surface passivation by carbonaceous deposits from impregnated organics impeded formation of significant amounts of $\text{Co}^{2+}_{(\text{Th})}$ in strong interaction with the alumina carrier. Absorptions beyond 700 nm in CAI and CAII could be due to $p(\text{O}^{2-}) \rightarrow e_g(\text{Co}^{3+})$ electronic transitions (Dhas et al., 2015).

Visible region signals around 400 nm in SA-containing formulations could be attributed to ligand to metal charge transfer (LMCT) complexes saccharide-molybdenum where Mo atoms could be partially reduced (Escobar et al., 2018). Similar absorptions due to LMCT complexes of thioglycolic acid-Mo have been previously identified by others (Toledo-Antonio et al., 2017; Palcheva et al., 2016). Position of bands due to those LMCT complexes depends upon Mo^{6+} and Mo^{5+} cations local symmetry related to their coordination and aggregation state (Zhong et al., 2018). Higher intensity of absorption at ~400 nm in SAI as to that in SAII spectrum suggested enhanced complex formation in the former. Signals at ~700 and ~867 nm related to Mo-blue species (Shukor et al., 2010) containing partially reduced molybdenum species (Escobar et al., 2018) were clearly identified in SA-modified samples. The former band (d-d transition) indicated partial Mo^{6+} reduction whereas the latter was originated by intervalent charge transfer Mo^{5+} to Mo^{6+} (Gavrilova et al., 2020). It has been mentioned that position of absorption maxima in the visible region could be related to shape of Mo-blue entities. Thus, peaks at around 750 nm could be due to ring-shaped toroidal species (Figure 3) whereas those at ~450 nm could be

characteristic of spherical ones (Müller et al., 1999). Then, in our SA-modified samples the latter species could be predominant. Strongly increased background absorption in visible range for SA-containing solids could be provoked by their dark coloring.

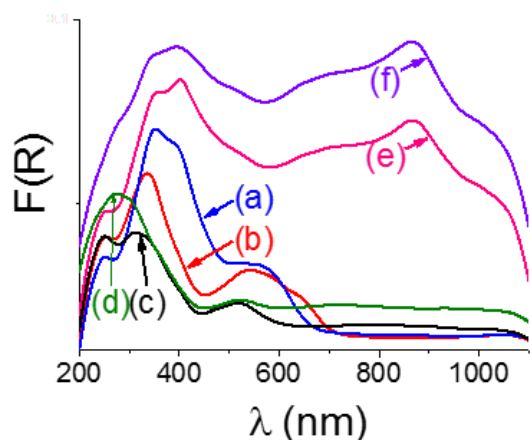


Figure 3. UV-vis DRS (Schuster-Kubelká-Munk function) spectra of alumina-supported P-doped CoMo oxidic materials prepared with and without organic additives. (a): CM_d; (b): CM_c; (c): CAI; (d): CAII; (e): SAI; (f): SAII.

Table 1. Absorptions maxima (nm) from UV-vis DRS (Schuster-Kubelká-Munk function) spectra of alumina-supported P-doped CoMo oxidic materials prepared with and without organic additives (Figure 3).

Sample	Mo ⁶⁺ _(Th)	Mo ⁶⁺ _(Oh)	Co ²⁺ _(Th)	Co ²⁺ _(Oh)	Mo-blue
CM _d	250	354, 396	560	521	
CM _c	254	335	540, 595, 645		
CAI	250	312		519, 785	
CAII	240	275		524, 722	
SAI	253	354		521	401, 692, 868
SAII	271	347		518	400, 700, 867

3.4. Temperature-programmed reduction of prepared formulations

Maxima of signals from TPR profiles (Figure 4) are summarized in Table 2. Low-temperature humps between 220-380 °C for CA-modified samples suggested evolution of products from decomposition of loosely bound organic additive. The corresponding broad signals in that temperature

range could be provoked by both alteration of the thermal conductivity detector by evolved species and some H₂ consumption as well (González-Cortés et al., 2015; Villareal et al., 2015).

Signals around 500 °C in various profiles were attributed to reduction of Mo⁶⁺_(Oh) in oxomolybdates to Mo⁴⁺, as previously reported in the case of γ-alumina-supported CoMo formulations of similar loading (Zhang et al., 2019). With the sole exception of SAI, the influence of organics addition on that signal position was no significant. The shift to higher temperature (520 °C) observed for that sample prepared by simultaneous SA + one-pot Co-Mo-P impregnating solution deposition agreed with increased LMCT complexes formation (Escobar et al., 2010), in agreement with that found by UV-vis spectroscopy (see section 3.3.). However, increased Mo⁶⁺_(Oh) dispersion in CA-modified samples (as suggested by blue-shifted absorption edge in UV-vis spectra, Figure 3) was not reflected in increased reduction temperature probably due to decreased Mo-alumina interaction provoked by support-like carbonaceous remains acting as intermediate carrier as proposed by others (Ge et al., 2014) from studies on ethylenediamine-modified CoMo/Al₂O₃ catalysts.

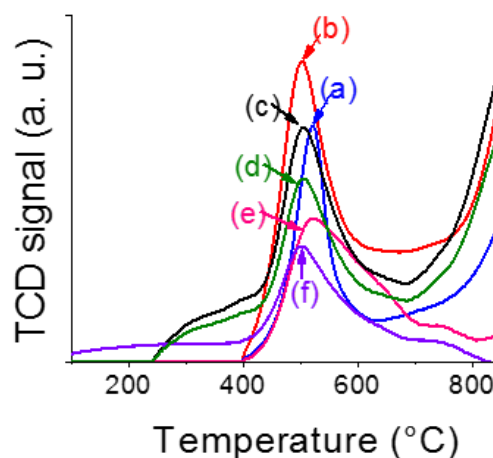


Figure 4. Temperature-programmed reduction profiles of alumina-supported P-doped CoMo oxidic impregnated materials prepared with and without organic additives. (a): CM_d; (b): CM_c; (c): CAI; (d): CAII; (e): SAI; (f): SAII.

Humps in the 708-750 °C range for studied samples could be related to reduction of Mo⁶⁺ in Al₂(MoO₄)₃ (Qu et al., 2003). Although those molybdates are favored by high-temperature annealing (migration to octahedral vacancies in the alumina structure) it seemed that impregnating by acidic Co-Mo-P solutions (pH~2) could partially dissolve the Al₂O₃ network that disruption provoking then aluminum molybdate formation in non-calcined samples.

Table 2. Maxima of signals from temperature-programmed reduction profiles of P-modified CoMo/Al₂O₃ materials prepared (Figure 4).

Sample	Mo ⁶⁺ _(OH) to Mo ⁴⁺	Co ²⁺ _(OH) to Co ⁰	Mo ⁶⁺ _(OH) in Al ₂ (MoO ₄) ₃ to Mo ⁰	Mo ⁶⁺ _(TH) to Mo ⁰
	(°C)	(°C)	(°C)	(°C)
CoMo _d	521	-	708 ^a	775 ^c
CoMo _c	502	-	726 ^a	770 ^c
CAI	504	648 ^a	727 ^b	772 ^c
CAII	504	645 ^a	733 ^b	772 ^c
SAI	520	615 ^b	750 ^a	-
SAII	500	639 ^b	745 ^a	-

^a: hump; ^b: shoulder; ^c: and beyond

Small H₂ consumption signals at 615-648 °C in solids containing organic additive could be provoked by reduction of Co²⁺ in tetrahedral vacancies of γ-Al₂O₃ phase to Co⁰ (Madduluri et al., 2019; Vosoughi et al., 2017). Shift of that peak to lower temperature in SAI (615 °C) suggested lessened Co-carrier interaction. On the other hand, absence of those consumptions in CoMo_d and CoMo_c TPR profiles could be due to hardly reducible Co²⁺_(TH) in cobalt aluminate domains, in full agreement with that found by UV-vis DRS (see Figure 3 and Table 1).

Signals at temperature beyond 770 °C in all samples (but in SA-modified ones) could include contributions from Mo⁴⁺ transformation to corresponding metallic phase and Mo⁶⁺_(TH) reduction of strongly interacting with the carrier (Escobar et al., 2017) as well. The most intense of those signals were observed for CAI and CM_c. For the latter, high temperature annealing (400 °C) at which the sample was submitted could favor stronger Mo-support interaction. In full agreement with that, CM_d (no submitted to calcining) had much lower H₂ consumption signal related to those refractory species reductions that could however exist as consequence of using acidic impregnating solutions, as previously mentioned. In the same line, when citric acid was directly added in the one-pot Co-Mo-P solution impregnating pH could slightly decrease leading to enhanced carrier dissolution. (Yin et al., 2011). Thus, proportion of refractory molybdenum could be augmented (see corresponding CAI profile in Figure 4). Absence of those Mo species in SA-modified solids points out to strong interaction of support with carbonaceous deposits that effectively passivated the alumina surface (Escobar et al., 2016). As the amount of C deposited on CA- and SA-modified solids was very similar (~0.072 g/g_{cat}) enhanced proportion of more stable graphitic support-like carbon (Escobar et al., 2018) in the latter formulations was strongly suggested.

3.5. Mo 3d XPS studies of oxidic impregnated formulations

Mo 3d spectra of various oxidic impregnated formulations dried at 120 °C (CM_c being sole exception as it was calcined at 400 °C) are shown in Figure 5.

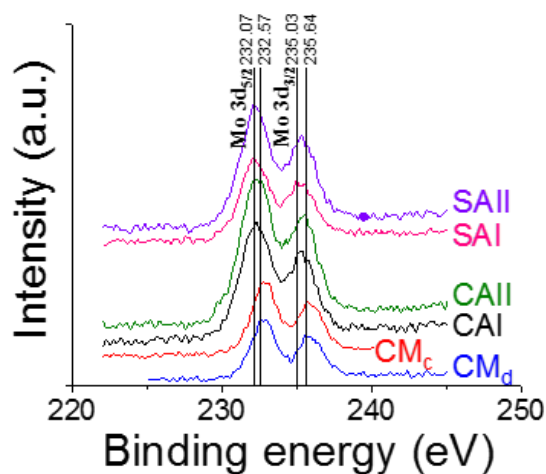


Figure 5. XPS Mo3d spectra of alumina-supported P-doped CoMo oxidic impregnated materials prepared with and without organic additives.

The Mo 3d spectrum of samples prepared with no organic additive (both dried and calcined, CM_d and CM_c, respectively) presented Mo 3d_{5/2} and Mo 3d_{3/2} doublet with binding energy of 232.57 and 235.64 eV, respectively, attributed to Mo⁶⁺ in oxomolybdates (Pimerzin et al., 2017). Wider full width at half maximum (FWHM) of Mo3d_{5/2} signal of SA- and CA-containing samples as to those of non-modified solids (CM_d and CM_c) (Figure 5) suggested existence of more than one type of Mo species. All materials prepared with organic additive showed maxima shifted to lower binding energy (Mo 3d_{5/2} and Mo 3d_{3/2} doublet at 232.07 and 235.03 eV, respectively) pointing out to contributions from partially reduced Mo⁵⁺ species. In full agreement, others (Koyun et al., 2017) identified Mo-blue XPS signals synthesized in materials prepared in one-step solid state technique using voltammetric method. Mo 3d_{5/2} and Mo 3d_{3/2} peaks (from Mo⁶⁺) at 232.98 and 236.08 eV, respectively, accompanied by contributions from Mo⁵⁺ at lower binding energy. Also, XPS signals related to partially reduced Mo⁵⁺ (additionally to those from Mo⁶⁺) have been identified (Chong et al., 2018) in [MoO₃(3,8-phenanthroline)_{0.5}] containing Mo-blue species where Mo 3d_{5/2} and Mo 3d_{3/2} peaks were observed at about 231.3 and 234.5 eV. Interestingly, presence of Mo⁵⁺ surface species was related to dark coloring

of samples, in full agreement with strongly increased background absorption in visible range for SA-containing samples (Figure 3).

In our case, shift to lower energy (Mo^{6+} to Mo^{5+}) was less pronounced in CAI where at the acidic conditions of impregnating solution (pH~2) citric acid could not be deprotonated in significant proportion (Escobar et al., 2017). Thus, interaction between Mo^{6+} species and organics could not be very strong as the organic acid could be largely unaltered. Partial molybdenum reduction (Mo^{5+} species) by either citric or malonic acid addition has been reported by others (Valencia et al., 2019) in the case of SiO_2 -supported molybdates obtained from ammonium heptamolybdate annealing. Presence of those Mo^{5+} (even some Mo^{4+}) species was attributed to organic acids oxidation by supported Mo^{6+} . In this case, however, no direct relationship between amount of partially reduced Mo species and activity in the palmitic acid HDO was found.

It is worth mentioning that interaction between molybdenum and citric acid could take place just after Co^{2+} complexes formation due to higher stability of the latter species at the concentrations (~ 2.5 and $\sim 1 \text{ mol l}^{-1}$ of Mo and Co, respectively) and pH conditions of impregnating solutions (Escobar et al., 2008; Sun et al., 2003). In prepared solutions used for Co-Mo-P one-pot simultaneous impregnation (as in CAI case, see section 2.1. Catalysts synthesis) cobalt cations could be preferably complexed over molybdenum ones. Thus, Mo entities reduction by CA could not be extensive in agreement with diminished Mo^{5+} species formation found by XPS (Figure 5). In full agreement, Mo complexation by CA was enhanced when the alumina bare support was first impregnated with citric acid in aqueous solution prior to Co-Mo-P phases deposition (CAII) where the organic modifier could possibly occupy coordinatively unsaturated sites (CUS, Al^{3+}) on Al_2O_3 carrier where several chelated Mo species could be identified (Escobar et al., 2017; Van Veen et al., 1989).

Regarding non chelating agents, Mo^{5+} species on dried alumina supported NiMo materials modified by ethylene glycol addition has been found (by XPS) (Nuzhdin et al., 2018), although no explanation for their existence was advanced in this case.

Respecting saccharide-modified solids our group has recently investigated on the effect of monosaccharides (from saccharose acid hydrolysis) as Mo^{+6} reductants which addition resulted in Mo-blue species formation (Escobar et al., 2018). Mo^{6+} (from $\text{P}_2\text{Mo}_5\text{O}_{23}^{6-}$ Strandberg heteropolyanions) reduction due to ligand to metal charge transfer (LMCT) complexes resulted in Mo-blue species that constituted suitable precursors of highly active alumina-supported sulfided NiMo HDS catalysts. Very interestingly, Mo^{5+} species from reduction of Mo^{6+} by using citric acid addition has been investigated on polymolybdates films (Jing et al., 2005) where

materials activated by UV irradiation (during 30 s) had signals related to electronic transitions forming strong symmetric band in the 500-900 nm region (maximum at $\lambda=670$ nm) induced by intervalence charge transfer (IVCT, $\text{Mo}^{5+} \leftrightarrow \text{Mo}^{6+}$) and d-d transitions of reduced polymolybdate species (Mo-blue) which presence was confirmed by XPS. In that study, absorption at 738 nm in visible region spectrum was assigned to $[\text{Mo}_{14}\text{O}_{46}]^{10-}$ species. In the same line, humps at 782 and 900 nm and at 720 and 865 nm in visible spectra of CAI and CAII, respectively (Figure 3) suggested extant partially reduced molybdenum species as well, as corroborated by corresponding XPS analyses (Figure 5). According to several reports, partially reduced Mo^{5+} species could play significant roles in HDO activity of corresponding Mo-based supported catalysts. For instance, improved catalytic activity (turn over frequency and stability) in the anisole HDO was related to active Mo oxide defects (e.g., Mo^{5+} species originated by post-synthesis treatment under H_2/CH_4 of ZrO_2 -supported oxidic Mo precursors) (Ranga et al., 2018). However, higher molybdenum reduction (to Mo^{4+}) resulted less favorable (Prasomsri et al., 2014). Mo^{5+} species generated by MoO_3 conversion either by carburization to $\text{MoO}_x\text{C}_y\text{H}_z$ or by reduction to MoO_{3-x} in presence of H_2 could be stabilized by lattice carbon preventing further reduction to Mo^{4+} by forming an oxycarbonyl phase (Prasomsri et al., 2014). Mo^{4+} -containing species as MoO_2 are completely inactive in phenolic species HDO (Prasomsri et al., 2014). On the other hand, Mo^{5+} species could presumably behave as Lewis acid sites (oxygen vacancies) that could weaken C-O bonds in molecules adsorbed on those active sites.

High activity and on-stream stability in the catalytic fast pyrolysis of lignocellulosic biomass was also observed in ZrO_2 - and TiO_2 -supported Mo (10 wt%) which contained over 50 wt% of partially reduced Mo species (Mo^{5+} and even Mo^{3+} in the material with titania as carrier) (Murugappan et al., 2016).

3.6. Sulfided catalysts characterization by high-resolution electron microscopy (HR-TEM)

From corresponding electron micrographs (Figure 6 (a)-(f)) some changes in MoS_2 particles morphology (slab length and stacking) of prepared sulfided catalysts by organics addition at different preparation stages were detected.

MoS_2 slabs average length of around 0.62 nm interplanar d -spacing (S-Mo-S layers in (002) plane) decreased, as to that in solids prepared with no organics, in materials modified by either CA or SA addition (Figure 7 (a) and (b) and Table 3).

Also, with the sole exception of SAII, for the rest of samples prepared with organic additive stacking degree slightly diminished respecting that found in either CM_d or CM_c formulations. SAI was the solid of the highest Mo^{4+} dispersion (D_{MoS_2} , from equation (5)) in full agreement with that previously reported (Escobar et al., 2018) where MoS_2 slab length

diminished in NiMo/alumina sulfided catalysts solids with saccharide addition. Interestingly, enhanced oxidic Mo dispersion in CAI and CAII as evidenced by hypsochromic shift in low-energy absorption edge in UV region (Figure 3) was preserved in corresponding sulfided solids.

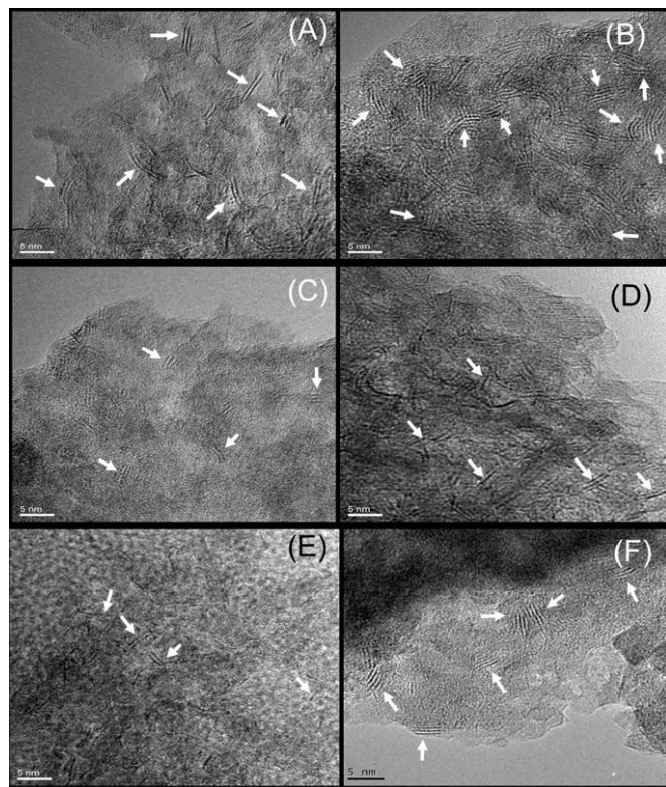


Figure 6. HR-TEM micrographs of various sulfided catalysts prepared with and without organic additives. White arrows: MoS₂ particles. (a) CM_d; (b) CM_c; (c): CAI; (d): CAII; (e): SAI; (f): SAII.

Weakened MoS₂-support interaction in SAII probably due to augmented amount of deposited carbon residua playing support-like role (Ge et al., 2014) resulted in longer slabs diminishing then Mo⁴⁺ dispersion (Table 3). CA-modified solids had similar MoS₂ particles morphology each other. Improved molybdenum sulfide slabs decoration by Co provoked by organic addition could significantly contribute to shortened slabs formation (Pimerzin et al., 2017). By using chelating agents that retarded low-temperature cobalt sulfidation MoS₂ slabs growth could be prevented. Promoter atoms could be fixed on MoS₂ edges after stable Co-complexes thermal decomposition (Nikulshin et al., 2014) once corresponding slabs had been already formed. On the other hand, in SA-modified solids carbonaceous residua could act as spacers hindering sulfided phases sintering thus improving

their dispersion (Escobar et al., 2018). Indeed, by thermal analysis it has been found that decomposition of blocking agents (carbonaceous deposits avoiding large clusters formation) and metal sulfidation processes could occur simultaneously explaining why non-complexing additives could delay promoters sulfidation thus enhancing CoMoS phase formation (Pimerzin et al., 2017). It is worth mentioning that decreased interaction between alumina carrier and deposited MoS₂ due to mentioned carbonaceous deposits could favor formation of so-called Type II sites (Nikulshin et al., 2012) characterized by significantly augmented HDS activity as to that of conventional Type I ones (Topsøe, 2007). Finally, it should be also considered that Mo-blue formation in solids prepared with saccharose could produce organic acids (by oxidation of fructose and glucose from saccharose hydrolysis) that could play the aforementioned role of chelating agents as Co sulfiding retardant (Nicosia & Prins, 2005b).

Table 3. Morphological properties of MoS₂ particles on various sulfided catalysts prepared (from statistical analyses shown in Figure 7 (a) and (b)).

Catalyst	^a L _{avg.} (nm)	^b D _{MoS₂}	^c N _{avg.}	^d A _r MoS ₂ (1/nm)	^e (f _e /f _c) _{MoS₂}
CM _d	3.84	0.30	4.3	1.12	4.50
CM _c	3.46	0.33	3.7	1.07	3.91
CAI	3.20	0.36	3.6	1.12	3.50
SAI	3.07	0.37	3.5	1.14	3.30
CAII	3.16	0.36	3.5	1.11	3.44
SAII	3.44	0.34	3.8	1.10	3.88

^aAverage slab length; ^b as estimated by Kasztelan model (Kasztelan et al., 1984) equation (5); ^c Average stacking; ^d Aspect ratio (from equation (3)); ^eMo (in MoS₂ slabs) edge-to-corner ratio from HR-TEM (equation (4))

SAI was the solid of the highest MoS₂ phase aspect ratio (A_rMoS₂, equation (3), Table 3) due to having the shortest average slab length (Shimada et al., 2016) that also provoked the lowest (f_e/f_c)_{MoS₂} = (Mo_e/Mo_c) ratio pointing out to enhanced number of corner sites in molybdenum sulfide slabs. Interestingly, it has been proposed that under HDS conditions, exposed metal atoms in corner sites could be resistant to inhibition by strongly adsorbed nitrogen-bearing compounds (Rangarajan et al., 2017). Thus, materials with augmented population of those sites (thus of smaller MoS₂ particles) could indeed be more active when hydrotreating real feedstocks containing aforementioned nitrogenated species. Also, it has been reported that MoS₂ particles morphology (slab length, stacking and aspect ratio) could play significant roles upon selectivity to different hydrotreating reactions (Fan et al., 2009).

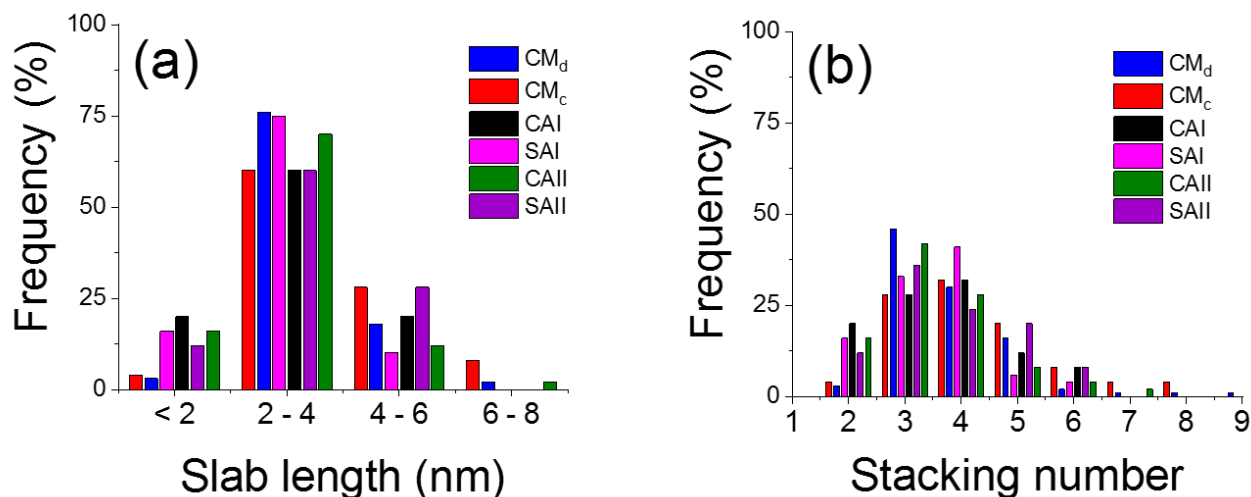


Figure 7. Statistical distribution of (a) length and (b) stacking of MoS₂ slabs over various sulfided catalysts prepared, as determined from corresponding HR-TEM micrographs.

Very interestingly sulfur-containing Mo-blue has been obtained by MoS₂ nanotubes exfoliation (Visic et al., 2013) where S 2p_{3/2} and 2p_{1/2} XPS peaks were identified at 169.2 and 170.4 eV being assigned to 4+ or 6+ valence states which could be related to SO₄⁻ or SO₃⁻ type species. That fact suggested that after catalysts activation (see section 2.1. Catalysts synthesis) some of those S-containing Mo-blue species could exist in our sulfided materials. Deeper insights in this aspect are needed.

Finally, catalytic test (activity and selectivity) of prepared organic agents-modified sulfided materials in the guayacol HDO and correlation of those data with the determined textural, structural and surface properties are in due course and will be presented in upcoming report. Interestingly, very good activity in the dimethylsulfide elimination through oxidative desulfurization to corresponding sulfoxide catalyzed by Mo-blue species has also been recently reported (Ratheshkumar et al., 2020). Also, Mo-blue has been applied as catalyst of enhanced activity and stability in the selective oxidation of cyclohexane to cyclohexanol and cyclohexanone (Liu et al., 2015). Catalysts containing “NiMoS” phases from alumina-supported Mo-blue precursors including partially reduced molybdenum species (Mo⁵⁺ entities) have shown very high activity in HDS reaction as well (Escobar et al., 2018).

4. Conclusions

Saccharose (SA) and citric acid (CA) were used as additives in P-doped CoMo/Al₂O₃ catalysts (Mo, Co and P at 12, 3, and 1.6 wt%, respectively). One-pot impregnating solutions were prepared by MoO₃ digestion in aqueous H₃PO₄, followed by cobalt acetate addition. Organics were integrated (SA/Co=1,

CA/Co=2) at two different preparation stages. During method I SA or CA was added in as-prepared Co-Mo-P one-pot impregnating solution, (pH~2) followed by pore-filling impregnation of alumina support whereas in method II prior to Co-Mo-P phases deposition SA or CA was impregnated on the pristine carrier, followed by drying (120 °C). Co-complexation by CA and Mo-blue (LMCT complex) formation (SA-modified solids) were identified by UV-vis analyses of corresponding oxidic dried samples. Also, partially reduced molybdenum species (Mo⁶⁺ => Mo⁵⁺, thus Mo-blue, by XPS) was observed after organics addition (either SA and CA) that effect being more evident in saccharose-modified solids. After sulfiding (H₂S/H₂ 10%, 400 °C, 2 h) Co-Mo-P phases impregnation in one-pot solution simultaneously deposited with SA rendered the materials of the highest MoS₂ dispersion (as determined by HR-TEM).

Conflict of interest

The authors have no conflict of interest to declare.

Acknowledgments

J. Escobar acknowledges IMP for supporting the investigation through D.61048 grant. A.W. Gutiérrez thanks CONACYT for her graduate student (doctorate) scholarship.

Financing

This investigation was funded through the D.061048 IMP grant.

References

- Beckett, S. T., Francesconi, M. G., Geary, P. M., Mackenzie, G., & Maulny, A. P. (2006). DSC study of sucrose melting. *Carbohydrate Research*, 341(15), 2591-2599.
<https://doi.org/10.1016/j.carres.2006.07.004>
- Blanchard, P., Payen, E., Grimblot, J., Le Bihan, L., Poulet, O., & Loutaty, R. (1998). Preparation of (Co)–Mo-based hydrodesulphurization catalysts: characterizations of deposited species on lanthanum modified γ -alumina. *Journal of Molecular Catalysis A: Chemical*, 135(2), 143-153.
[https://doi.org/10.1016/S1381-1169\(97\)00299-9](https://doi.org/10.1016/S1381-1169(97)00299-9)
- Braun, S., Appel, L. G., & Schmal, M. (2005). Molybdenum species on alumina and silica supports for soot combustion. *Catalysis Communications*, 6(1), 7-12.
<https://doi.org/10.1016/j.catcom.2004.10.002>
- Bui, V.N., Toussaint, G., Laurenti, D., Mirodatos, C., & Geantet, C. (2009). Co-processing of pyrolysis bio oils and gas oil for new generation of bio-fuels: Hydrodeoxygenation of guaiacol and SRGO mixed feed. *Catalysis Today*, 143, 172-178.
<https://doi.org/10.1016/j.cattod.2008.11.024>
- Bui, V.N., Laurenti, D., Delichère, P., & Geantet, C. (2011a). Hydrodeoxygenation of guaiacol Part II: Support effect for CoMoS catalysts on HDO activity and selectivity. *Applied Catalysis B: Environmental*, 101, 245-255.
<https://doi.org/10.1016/j.apcatb.2010.10.031>
- Bui, V.N., Laurenti, D., Afanasiev, P., & Geantet, C. (2011b). Hydrodeoxygenation of guaiacol with CoMo catalysts. Part I: Promoting effect of cobalt on HDO selectivity and activity. *Applied Catalysis B: Environmental*, 101, 239-245.
<https://doi.org/10.1016/j.apcatb.2010.10.025>
- Catita, L., Quoineaud, A. A., Espinat, D., Pichon, C., & Delpoux, O. (2017). Application of magnetic resonance imaging and raman imaging to study the impact of phosphorus in impregnation of hydrotreatment catalysts. *Applied Catalysis A: General*, 547, 164-175.
<https://doi.org/10.1016/j.apcata.2017.08.039>
- Chio, C., Sain, M., & Qin, W. (2019). Lignin utilization: a review of lignin depolymerization from various aspects. *Renewable and Sustainable Energy Reviews*, 107, 232-249.
<https://doi.org/10.1016/j.rser.2019.03.008>
- Chong, S. V., Jameson, G. B., Waterland, M. R., & Tallon, J. L. (2018). Evidence of reduced species in molybdenum oxide-phenanthroline layered hybrids from structural, magnetic and X-ray photoelectron spectroscopy studies. *Materials Letters*, 231, 187-189.
<https://doi.org/10.1016/j.matlet.2018.08.039>
- Dhas, C. R., Venkatesh, R., Jothivenkatachalam, K., Nithya, A., Benjamin, B. S., Raj, A. M. E., & Sanjeeviraja, C. (2015). Visible light driven photocatalytic degradation of Rhodamine B and Direct Red using cobalt oxide nanoparticles. *Ceramics International*, 41(8), 9301-9313.
<https://doi.org/10.1016/j.ceramint.2015.03.238>
- Eggleston, G., Trask-Morrell, B. J., & Vercellotti, J. R. (1996). Use of differential scanning calorimetry and thermogravimetric analysis to characterize the thermal degradation of crystalline sucrose and dried sucrose-salt residues. *Journal of Agricultural and Food Chemistry*, 44(10), 3319-3325.
<https://doi.org/10.1021/jf950836z>
- Escobar, J., De los Reyes, J. A., & Viveros, T. (2000). Influence of the synthesis additive on the textural and structural characteristics of sol-gel Al_2O_3 - TiO_2 . *Industrial & engineering chemistry research*, 39(3), 666-672.
<https://doi.org/10.1021/ie990487o>
- Escobar, J., Barrera, M. C., De los Reyes, J. A., Toledo, J. A., Santes, V., & Colín, J. A. (2008). Effect of chelating ligands on Ni–Mo impregnation over wide-pore ZrO_2 - TiO_2 . *Journal of molecular catalysis A: Chemical*, 287(1-2), 33-40.
<https://doi.org/10.1016/j.molcata.2008.02.022>
- Escobar, J., Barrera, M. C., Toledo, J. A., Cortés-Jácome, M. A., Angeles-Chavez, C., Núñez, S., & Pacheco, J. G. (2009). Effect of ethyleneglycol addition on the properties of P-doped NiMo/ Al_2O_3 HDS catalysts: Part I. Materials preparation and characterization. *Applied Catalysis B: Environmental*, 88(3-4), 564-575.
<https://doi.org/10.1016/j.apcatb.2008.10.005>
- Escobar, J., Toledo, J. A., Gutiérrez, A. W., Barrera, M. C., Cortés, M. A., Angeles, C., & Díaz, L. (2010). Enhanced dibenzothiophene desulfurization over NiMo catalysts simultaneously impregnated with saccharose. In *Studies in Surface Science and Catalysis*, 175, 767-770. Elsevier.
[https://doi.org/10.1016/S0167-2991\(10\)75156-9](https://doi.org/10.1016/S0167-2991(10)75156-9)

- Escobar, J., Gutiérrez, A. W., Barrera, M. C., & Colín, J. A. (2016). NiMo/alumina hydrodesulphurization catalyst modified by saccharose: Effect of addition stage of organic modifier. *The Canadian Journal of Chemical Engineering*, 94(1), 66-74.
<https://doi.org/10.1002/cjce.22334>
- Escobar, J., Barrera, M. C., Gutiérrez, A. W., & Terrazas, J. E. (2017). Benzothiophene hydrodesulfurization over NiMo/alumina catalysts modified by citric acid. Effect of addition stage of organic modifier. *Fuel Processing Technology*, 156, 33-42.
<https://doi.org/10.1016/j.fuproc.2016.09.028>
- Escobar, J., Barrera, M. C., Gutiérrez, A. W., Cortés-Jacome, M. A., Angeles-Chávez, C., Toledo, J. A., & Solís-Casados, D. A. (2018). Highly active P-doped sulfided NiMo/alumina HDS catalysts from Mo-blue by using saccharose as reducing agents precursor. *Applied Catalysis B: Environmental*, 237, 708-720.
<https://doi.org/10.1016/j.apcatb.2018.06.034>
- Fagerson, I. S. (1969). Thermal degradation of carbohydrates; a review. *Journal of Agricultural and Food Chemistry*, 17(4), 747-750.
<https://doi.org/10.1021/jf60164a019>
- Fan, Y., Shi, G., Liu, H., & Bao, X. (2009). Morphology tuning of supported MoS₂ slabs for selectivity enhancement of fluid catalytic cracking gasoline hydrodesulfurization catalysts. *Applied Catalysis B: Environmental*, 91(1-2), 73-82.
<https://doi.org/10.1016/j.apcatb.2009.05.008>
- Gavrilova, N., Myachina, M., Harlamova, D., & Nazarov, V. (2020). Synthesis of molybdenum blue dispersions using ascorbic acid as reducing agent. *Colloids and Interfaces*, 4(2), 24.
<https://doi.org/10.3390/colloids4020024>
- Ge, H., Wen, X. D., Ramos, M. A., Chianelli, R. R., Wang, S., Wang, J., & Li, X. (2014). Carbonization of ethylenediamine coimpregnated CoMo/Al₂O₃ catalysts sulfided by organic sulfiding agent. *ACS Catalysis*, 4(8), 2556-2565.
<https://doi.org/10.1021/cs500477x>
- González-Cortés, S. L., Qian, Y., Almegren, H. A., Xiao, T., Kuznetsov, V. L., & Edwards, P. P. (2015). Citric acid-assisted synthesis of γ -alumina-supported high loading CoMo sulfide catalysts for the hydrodesulfurization (HDS) and hydrodenitrogenation (HDN) reactions. *Applied Petrochemical Research*, 5(3), 181-197.
<https://doi.org/10.1007/s13203-015-0097-y>
- Grimes, R. W., & Fitch, A. N. (1991). Thermal decomposition of cobalt (II) acetate tetrahydrate studied with time-resolved neutron diffraction and thermogravimetric analysis. *Journal of Materials Chemistry*, 1(3), 461-468.
<https://doi.org/10.1039/JM9910100461>
- Humbert, S., Devers, E., Lesage, C., Legens, C., Lemaitre, L., Sorbier, L., & Briois, V. (2021). ASAXS study of the influence of sulfidation conditions and organic additives on sulfide slabs multiscale organization. *Journal of Catalysis*, 395, 412-424.
<https://doi.org/10.1016/j.jcat.2021.01.033>
- Jing, W., Guang-Jin, Z., Wen-Sheng, Y., & Jian-Nian, Y. (2005). Multicolor Photochromism of Polymolybdate-Citric Acid Composite Films. *Chinese Journal of Chemistry*, 23(8), 1037-1041.
<https://doi.org/10.1002/cjoc.200591037>
- Kaluža, L., Karban, J., & Gulková, D. (2019). Activity and selectivity of Co (Ni) Mo sulfides supported on MgO, Al₂O₃, ZrO₂, TiO₂, MCM-41 and activated carbon in parallel hydrodeoxygenation of octanoic acid and hydrodesulfurization of 1-benzothiophene. *Reaction Kinetics, Mechanisms and Catalysis*, 127(2), 887-902.
<https://doi.org/10.1007/s11144-019-01620-x>
- Kasztelan, S., Toulhoat, H., Grimblot, J., & Bonnelle, J. P. (1984). A geometrical model of the active phase of hydrotreating catalysts. *Applied Catalysis*, 13(1), 127-159.
[https://doi.org/10.1016/S0166-9834\(00\)83333-3](https://doi.org/10.1016/S0166-9834(00)83333-3)
- Koyun, O., Gorduk, S., Arvas, M. B., & Sahin, Y. (2017). Direct, one-step synthesis of molybdenum blue using an electrochemical method, and characterization studies. *Synthetic Metals*, 233, 111-118.
<http://doi.org/10.1016/j.synthmet.2017.09.009>
- Kraus, H., & Prins, R. (1996). Composition of Impregnation Solutions and Wet Impregnated Mo-P/ γ -Al₂O₃ Catalysts as Investigated by ³¹P and ⁹⁵Mo NMR. *Journal of Catalysis*, 164(2), 251-259.
<https://doi.org/10.1006/jcat.1996.0381>
- Lee, H., Kim, H., Yu, M. J., Ko, C. H., Jeon, J. K., Jae, J., & Park, Y. K. (2016). Catalytic hydrodeoxygenation of bio-oil model compounds over Pt/HY catalyst. *Scientific reports*, 6(1), 1-8.
<https://doi.org/10.1038/srep28765>

- Lélias, M. A., Kooyman, P. J., Marley, L., Oliviero, L., Travert, A., Van Gestel, J., & Mauge, F. (2009). Effect of NTA addition on the structure and activity of the active phase of cobalt-molybdenum sulfide hydrotreating catalysts. *Journal of Catalysis*, 267(1), 14-23.
<https://doi.org/10.1016/j.jcat.2009.07.006>
- Leofanti, G., Padovan, M., Tozzola, G., & Venturelli, B. J. C. T. (1998). Surface area and pore texture of catalysts. *Catalysis today*, 41(1-3), 207-219.
[https://doi.org/10.1016/S0920-5861\(98\)00050-9](https://doi.org/10.1016/S0920-5861(98)00050-9)
- Lin, Y.C., Li, C.-L., Wan, H.-P., Lee, H.T., & Liu, C.-F. (2011). Catalytic Hydrodeoxygenation of Guaiacol on Rh-Based and Sulfided CoMo and NiMo Catalysts. *Energy Fuels*, 25, 890-896.
<https://doi.org/10.1021/ef101521z>
- Li, C., Zhao, X., Wang, A., Huber, G. W., & Zhang, T. (2015). Catalytic transformation of lignin for the production of chemicals and fuels. *Chemical reviews*, 115(21), 11559-11624.
<https://doi.org/10.1021/acs.chemrev.5b00155>
- Liu, X., Conte, M., Weng, W., He, Q., Jenkins, R. L., Watanabe, M., & Hutchings, G. J. (2015). Molybdenum blue nano-rings: an effective catalyst for the partial oxidation of cyclohexane. *Catalysis Science & Technology*, 5(1), 217-227.
<https://doi.org/10.1039/C4CY01213E>
- Liu, Y., Wu, K., Guo, X. I., Wang, W.Y., & Yang, Y. Q. (2018). A comparison of MoS₂ catalysts hydrothermally synthesized from different sulfur precursors in their morphology and hydrodeoxygenation activity. *Journal of Fuel Chemistry and Technology*, 46(5), 535-542.
[https://doi.org/10.1016/S1872-5813\(18\)30023-9](https://doi.org/10.1016/S1872-5813(18)30023-9)
- Madduluri, V. R., & Rao, K. S. R. (2019). Advantage of Co embedded γ -Al₂O₃ catalysts over MgO and SiO₂ solid oxides in the selective production of styrene monomer. *Catalysis Letters*, 149(11), 3238-3252.
<https://doi.org/10.1007/s10562-019-02903-7>
- Müller, A., Sarkar, S., Shah, S. Q. N., Bögge, H., Schmidtman, M., Sarkar, S., & Schünemann, V. (1999). Archimedean synthesis and magic numbers: "sizing" giant molybdenum-oxide-based molecular spheres of the keplerate type. *Angewandte Chemie International Edition*, 38(21), 3238-3241.
[https://doi.org/10.1002/\(SICI\)15213773\(19991102\)38:21<3238::AID-ANIE3238>3.0.CO;2-6](https://doi.org/10.1002/(SICI)15213773(19991102)38:21<3238::AID-ANIE3238>3.0.CO;2-6)
- Murugappan, K., Mukarakate, C., Budhi, S., Shetty, M., Nimlos, M. R., & Román-Leshkov, Y. (2016). Supported molybdenum oxides as effective catalysts for the catalytic fast pyrolysis of lignocellulosic biomass. *Green Chemistry*, 18(20), 5548-5557.
<https://doi.org/10.1039/C6GC01189F>
- Nicosia, D., & Prins, R. (2005a). The effect of glycol on phosphate-doped CoMo/Al₂O₃ hydrotreating catalysts. *Journal of Catalysis*, 229(2), 424-438.
<https://doi.org/10.1016/j.jcat.2004.11.014>
- Nicosia, D., & Prins, R. (2005b). The effect of phosphate and glycol on the sulfidation mechanism of CoMo/Al₂O₃ hydrotreating catalysts: an in situ QEXAFS study. *Journal of Catalysis*, 231(2), 259-268.
<https://doi.org/10.1016/j.jcat.2005.01.018>
- Nikulshin, P. A., Mozhaev, A. V., Pimerzin, A. A., Konovalov, V. V., & Pimerzin, A. A. (2012). CoMo/Al₂O₃ catalysts prepared on the basis of Co₂Mo₁₀-heteropolyacid and cobalt citrate: effect of Co/Mo ratio. *Fuel*, 100, 24-33.
<https://doi.org/10.1016/j.fuel.2011.11.028>
- Nikulshin, P.A., Ishutenko, D.I., Mozhaev, A.A., Maslakov, K.I., & Pimerzin, A.A. (2014). Effects of composition and morphology of active phase of CoMo/Al₂O₃ catalysts prepared using Co₂Mo₁₀-heteropolyacid and chelating agents on their catalytic properties in HDS and HYD reactions. *Journal of catalysis*, 312, 152-169.
<https://doi.org/10.1016/j.jcat.2014.01.014>
- Nuzhdin, A.L., Vlasova, E.N., Bukhtiyarova, G.A., Porsin, A.A., Prosvirin, I.P., & Bukhtiyarov, V.I. (2018). Beneficial effect of ethylene glycol on the activity of P-doped NiMo/Al₂O₃ HDS catalysts, *WSEAS Transactions on Environment and Development*, 14, 630-635.
- Őrsi, F. (1973). Kinetic studies in the thermal decomposition of glucose and fructose. *Journal of thermal analysis*. 5, 329-335.
<https://doi.org/10.1007/BF01950381>
- Palcheva, R., Kaluža, L., Dimitrov, L., Tyuliev, G., Avdeev, G., Jirátoová, K., & Spojakina, A. (2016). NiMo catalysts supported on the Nb modified mesoporous SBA-15 and HMS: effect of thioglycolic acid addition on HDS. *Applied Catalysis A: General*, 520, 24-34.
<https://doi.org/10.1016/j.apcata.2016.04.008>
- Pimerzin, A., Mozhaev, A., Varakin, A., Maslakov, K., & Nikulshin, P. (2017). Comparison of citric acid and glycol effects on the state of active phase species and catalytic properties of CoPMo/Al₂O₃ hydrotreating catalysts. *Applied Catalysis B: Environmental*, 205, 93-103.
<https://doi.org/10.1016/j.apcatb.2016.12.022>

- Prasomsri, T., Shetty, M., Murugappan, K., & Roman-Leshkov, Y. (2014). Insights into the catalytic activity and surface modification of MoO₃ during the hydrodeoxygenation of lignin-derived model compounds into aromatic hydrocarbons under low hydrogen pressures. *Energy & Environmental Science*, 7, 2660-2669.
<https://doi.org/10.1039/C4EE00890A>
- Qi, Z., Jie, C., Tiejun, W., & Ying, X. (2007). Review of biomass pyrolysis oil properties and upgrading Research. *Energy Conver. Manag.*, 48(1), 87-92.
<https://doi.org/10.1016/j.enconman.2006.05.010>
- Qu, L., Zhang, W., Kooyman, P. J., & Prins, R. (2003). MAS NMR, TPR, and TEM studies of the interaction of NiMo with alumina and silica-alumina supports. *Journal of Catalysis*, 215(1), 7-13.
[https://doi.org/10.1016/S0021-9517\(02\)00181-1](https://doi.org/10.1016/S0021-9517(02)00181-1)
- Ramírez, J., Contreras, R., Castillo, P., Klimova, T., Zárate, R., & Luna, R. (2000). Characterization and Catalytic Activity of CoMo HDS Catalysts Supported on Alumina-MCM-41. *Applied Catalysis A: General*, 197, 69-78.
[https://doi.org/10.1016/S0926-860X\(99\)00534-7](https://doi.org/10.1016/S0926-860X(99)00534-7)
- Ranga, C., Lødeng, R., Alexiadis, V. I., Rajkhowa, T., Bjørkan, H., Chytil, S., & Thybaut, J. W. (2018). Effect of composition and preparation of supported MoO₃ catalysts for anisole hydrodeoxygenation. *Chemical Engineering Journal*, 335, 120-132.
<https://doi.org/10.1016/j.cej.2017.10.090>
- Rangarajan, S., & Mavrikakis, M. (2017). On the Preferred Active Sites of Promoted MoS₂ for Hydrodesulfurization with Minimal Organonitrogen Inhibition. *ACS Catalysis*, 7(1), 501-509.
<https://doi.org/10.1021/acscatal.6b02735>
- Ratheshkumar, P., Induja, S., Ravishankar, R., & Raghavan, P.S. (2020). One-step synthesis of thermally stable solid molybdenum blue using boron phosphate. *Rasayan J. Chem.*, 13 (2), 803-809.
- Rinaldi, N., Kubota, T., & Okamoto, Y. (2009). Effect of Citric Acid Addition on Co-Mo/B₂O₃/Al₂O₃ Catalysts Prepared by a Post-Treatment Method. *Industrial & engineering chemistry research*, 48, 10414-10424.
<https://doi.org/10.1021/ie9008343>
- Shimada, H. (2016). Morphology, Dispersion and Catalytic functions of Molybdenum Sulfide Catalysts for Hydrotreating Petroleum Fractions. *Journal of the Japan Petroleum Institute*, 59, 46-58.
<https://doi.org/10.1627/jpi.59.46>
- Shukor, M.Y., Rahman, M.F., Suhaili, Z., Shamaan, N.A., & Syed, M.A. (2010). Hexavalent Molybdenum Reduction to Mo-blue by *Acinetobacter calcoaceticus*. *Folia Microbiologica*, 55 (2), 137-143.
<https://doi.org/10.1007/s12223-010-0021-x>
- Stampfl, S. R., Chen, Y., Dumesic, J. A., Niu, C., & Hill Jr, C. G. (1987). Interactions of molybdenum oxide with various oxide supports: Calcination of mechanical mixtures. *Journal of catalysis*, 105(2), 445-454.
[https://doi.org/10.1016/0021-9517\(87\)90072-8](https://doi.org/10.1016/0021-9517(87)90072-8)
- Stevulova, N., Estokova, A., Cigasova, J., Schwarzova, I., Kacik, F., & Geffert, A. (2017). Thermal degradation of natural and treated hemp hurds under air and nitrogen atmosphere. *Journal of Thermal Analysis and Calorimetry*, 128(3), 1649-1660.
<https://doi.org/10.1007/s10973-016-6044-z>
- Sun, M., Nicosia, D., & Prins, R. (2003). The effects of fluorine, phosphate and chelating agents on hydrotreating catalysts and catalysis. *Catalysis Today*, 86(1-4), 173-189.
[https://doi.org/10.1016/S0920-5861\(03\)00410-3](https://doi.org/10.1016/S0920-5861(03)00410-3)
- Tavizón-Pozos, J.A., Santolalla-Vargas, C.E., Valdés-Martínez, O.U., & De los Reyes Heredia, J.A. (2019). Effect of Metal Loading in Unpromoted and Promoted CoMo/Al₂O₃-TiO₂ Catalysts for the Hydrodeoxygenation of Phenol. *Catalysts*, 9 (6), 550.
<https://doi.org/10.3390/catal9060550>
- Toledo-Antonio, J.A., Cortés-Jácome, M.A., Escobar-Aguilar, J., Angeles-Chavez, C., Navarrete-Bolaños, J., & López-Salinas, E. (2017). Upgrading HDS activity of MoS₂ by thioglycolic acid complex with MoO_x supported on the alumina *Applied Catalysis B: Environmental*, 213, 106-117.
<https://doi.org/10.1016/j.apcatb.2017.05.011>
- Topsøe, H. (2007). The role of Co-Mo-S type structures in hydrotreating catalysts. *Applied Catalysis A: General*, 322, 3-8.
<https://doi.org/10.1016/j.apcata.2007.01.002>
- Valencia, D., Díaz, I., Ramírez-Verduzco, L.F., Amezcua-Allieri, M.A., & Aburto, J. (2019). MoO₃-based catalysts supported on SiO₂ and their performance in hydrodeoxygenation, *Materials Letters*, 251, 226-229.
<https://doi.org/10.1016/j.matlet.2019.05.075>
- van Haandel, L., Bremmer, G.M., Hensen, E.J.M., & Weber, Th. (2017). The effect of organic additives and phosphoric acid on sulfidation and activity of (Co)Mo/Al₂O₃ hydrodesulfurization catalysts. *Journal of Catalysis*, 351, 95-106.
<https://doi.org/10.1016/j.jcat.2017.04.012>

- Van Veen, J. R., Jonkers, G., & Hesselink, W. H. (1989). Interaction of Transition-metal Acetylacetonates with γ - Al_2O_3 Surfaces. *Journal of the Chemical Society, Faraday Transactions 1: Physical Chemistry in Condensed Phases*, 85(2), 389-413.
<https://doi.org/10.1039/F19898500389>
- Vatutina, Y.V., Kazakova, M.A., Gerasimov, E.Y., Prosvirin, I.P., Klimov, O.V., Noskov, A.S., & Kazakov, M.O. (2020). Effect of Organic Additives on the Structure and Hydrotreating Activity of a CoMoS/Multiwalled Carbon Nanotube Catalyst. *Industrial & Engineering Chemistry Research*, 59(47), 20612-20623.
<https://doi.org/10.1021/acs.iecr.0c03915>
- Villarreal, A., Ramírez, J., Cedeño Caero, L., Castillo Villalón, P., & Gutiérrez-Alejandre, A. (2015). Importance of the sulfidation step in the preparation of highly active NiMo/SiO₂/Al₂O₃ hydrodesulfurization catalysts. *Catalysis Today*, 250, 60-65.
<https://doi.org/10.1016/j.cattod.2014.03.035>
- Visic, B., Klanjek Gunde, M., Kovac, J., Iskra, I., Jelenc, J., & Remskar, M. (2013). MoS₂ nanotube exfoliation as new synthesis pathway to molybdenum blue. *Materials Research Bulletin*, 48(2), 802-806.
<https://doi.org/10.1016/j.materresbull.2012.11.062>
- Vosoughi, V., Badoga, S., Dalai, A.K., & Abatzoglou, N. (2017). Modification of mesoporous alumina as a support for cobalt-based catalyst in Fischer-Tropsch synthesis. *Fuel Processing Technology*, 162, 55-65.
<https://doi.org/10.1016/j.fuproc.2017.03.029>
- Weber, R.S. (1995). Effect of local structure on the UV-visible absorption edges of molybdenum oxide clusters and supported molybdenum oxides. *Journal of Catalysis*, 151(2), 470-474.
<https://doi.org/10.1006/jcat.1995.1052>
- Wu, K., Wang, W., Tan, S., Zhu, G., Tan, L., & Yang, Y. (2016). Microwave-assisted hydrothermal synthesis of amorphous MoS₂ catalysts and their activities in the hydrodeoxygenation of p-cresol. *RSC advances*, 6(84), 80641-80648.
<https://doi.org/10.1039/C6RA19007C>
- Wu, K., Wang, C., Chen, X., Wang, W., & Yang, Y. (2019). Facile synthesis of hydrophobic MoS₂ and its activity and stability in the hydrodeoxygenation reaction. *New Journal of Chemistry*, 43(6), 2734-2739.
<https://doi.org/10.1039/C8NJ05980B>
- Xie, L. L., Gao, Q. M., & Li, Q. H. (2007). Nanoporous metal phosphate CoVSB-1 catalyst for oxidation of styrene with H₂O₂. In *Studies in surface science and catalysis* (Vol. 170, pp. 1338-1343).
[https://doi.org/10.1016/S0167-2991\(07\)80997-9](https://doi.org/10.1016/S0167-2991(07)80997-9)
- Yang, Y. Q., Tye, C. T., & Smith, K. J. (2008). Influence of MoS₂ catalyst morphology on the hydrodeoxygenation of phenols. *Catalysis Communications*, 9(6), 1364-1368.
<https://doi.org/10.1016/j.catcom.2007.11.035>
- Yin, H.I., Zhou, T. N., Liu Y. Q., Chai, Y. M, & Liu, C.G. (2011). Study on the structure of active phase in NiMoP impregnation solution using Laser Raman spectroscopy II. Effect of organic additives. *Journal of Fuel Chemistry and Technology*, 39(2), 109-114.
[https://doi.org/10.1016/S1872-5813\(11\)60012-1](https://doi.org/10.1016/S1872-5813(11)60012-1)
- Zhang, C., Brorson, M., Li, P., Liu, X., Liu, T., Jiang, Z., & Li C. (2019). CoMo/Al₂O₃ catalysts prepared by tailoring the surface properties of alumina for highly selective hydrodesulfurization of FCC gasoline. *Applied Catalysis A: General*, 570, 84-95.
<https://doi.org/10.1016/j.apcata.2018.10.039>
- Zheng, M., Zhao, L., Cao, L., Zhang, Y., Gao, J., & Xu, C. (2021). Insights into the HDS/HYDO selectivity with considering stacking effect of Co-MoS₂ catalysts by combined DFT and microkinetic method. *Fuel*, 300, 120941.
<https://doi.org/10.1016/j.fuel.2021.120941>
- Zhong, W., Liu, M., Dai, J., Yang, J., Mao, L., & Yin, D. (2018). Synergistic hollow CoMo oxide dual catalysis for tandem oxygen transfer: Preferred aerobic epoxidation of cyclohexene to 1,2-epoxycyclohexane. *Applied Catalysis B: Environmental*, 225, 180-196.
<https://doi.org/10.1016/j.apcatb.2017.11.074>